ACS Catalysis

Freie Universität Berlin

Subscriber access provided by UB + Fachbibliothek Chemie | (FU-Bibliothekssystem)

Article

The Geometry of the Catalytic Active Site in [FeFe]-hydrogenases is Determined by Hydrogen Bonding and Proton Transfer

JIFU DUAN, Stefan Mebs, Moritz Senger, Konstantin Laun, Florian Wittkamp, Joachim Heberle, Thomas Happe, Eckhard Hofmann, Ulf-Peter Apfel, Martin Winkler, Michael Haumann, and Sven T. Stripp

ACS Catal., **Just Accepted Manuscript** • DOI: 10.1021/acscatal.9b02203 • Publication Date (Web): 29 Aug 2019

The Geometry of the Catalytic Active Site in [FeFe]-hydrogenases is Determined by Hydrogen Bonding and Proton Transfer

Jifu Duan[1], Stefan Mebs[2], Moritz Senger[3], Konstantin Laun[3], Florian Wittkamp[4], Joachim Heberle[3], Thomas Happe[1], Eckhard Hofmann[5], Ulf-Peter Apfel[4,6], Martin Winkler[1], Michael Haumann[2], and Sven T. Stripp[3]*

[1] Faculty of Biology and Biotechnology, Photobiotechnology, Ruhr-University Bochum, 44801 Bochum, Germany

[2] Department of Physics, Biophysics of Metalloenzymes, Freie Universität Berlin, 14195 Berlin, Germany

[3] Department of Physics, Experimental Molecular Biophysics, Freie Universität Berlin, 14195 Berlin, Germany

[4] Faculty of Chemistry and Biochemistry, Inorganic Chemistry I, Ruhr University Bochum, 44801 Bochum, Germany

[5] Faculty of Biology and Biotechnology, Protein Crystallography, Ruhr University Bochum, 44801 Bochum, Germany

[6] Fraunhofer UMSICHT, 46047 Oberhausen, Germany

*Correspondence to:

Sven T. Stripp, Freie Universität Berlin, Fachbereich Physik, Arnimallee 14, 14195 Berlin, Germany, Phone: +49 30 838 55069, Email: sven.stripp@fu-berlin.de

ABSTRACT

[FeFe]-hydrogenases are efficient metalloenzymes that catalyze the oxidation and evolution of molecular hydrogen, H_2. They serve as a blueprint for the design of synthetic H_2-forming catalysts. [FeFe]-hydrogenases harbor a six-iron cofactor that comprises a [4Fe-4S] cluster and a unique diiron site with cyanide, carbonyl, and hydride ligands. To address the ligand dynamics in catalytic turnover and upon carbon monoxide (CO) inhibition, we replaced the native aminodithiolate group of the diiron site by synthetic dithiolates, inserted into wild-type and amino acid variants of the [FeFe]-hydrogenase HYDA1 from *Chlamydomonas reinhardtii*. The reactivity with H_2 and CO was characterized using *in situ* and transient infrared spectroscopy, protein crystallography, quantum chemical calculations, and kinetic simulations. All cofactor variants adopted characteristic populations of reduced species in the presence of H_2 and showed significant changes in CO inhibition and reactivation kinetics. Differences were attributed to varying interactions between polar ligands and the dithiolate head group and/or the environment of the cofactor (i.e., amino acid residues and water molecules). The presented results show how catalytically relevant intermediates are stabilized by inner-sphere hydrogen bonding suggesting that the role of the aminodithiolate group must not be restricted to proton transfer. These concepts may inspire the design of improved enzymes and biomimetic H_2-forming catalysts.

Keywords: metalloenzymes, cofactor dynamics, infrared spectroscopy, protein crystallography, quantum chemistry

INTRODUCTION

Hydrogenases are metalloenzymes that catalyze the reversible reduction of protons to molecular hydrogen (H_2).[1] They have been found in all domains of life participating in cellular energy metabolism and hydrogen sensing. Three different classes were identified: [FeFe]-hydrogenases catalyze both proton reduction and H_2 oxidation, e.g. in bacteria and algae, while [NiFe]- and [Fe]-hydrogenases are predominantly H_2-oxidizing enzymes in bacteria and archaea. Hydrogenase activity is reversibly inhibited by carbon monoxide (CO) usually impaired by molecular oxygen (O_2).[2–5] Here, the reactivity of [FeFe]-hydrogenases with CO and/or H_2 was employed to unravel molecular interactions involved in structural dynamics and catalytic performance at the active site.

The active site cofactor of [FeFe]-hydrogenases (H-cluster) comprises a unique diiron site covalently linked to a [4Fe-4S] cluster *via* a single cysteine (Fig. 1).[6–8] The *proximal* and *distal* iron ions of the diiron site (Fe_p, Fe_d) carry a single CO and cyanide (CN^-) ligand each and share a *bridging* carbonyl (μCO) in the oxidized resting state, **Hox**.[5,9] An open *apical* coordination site at Fe_d characterizes the so-called "rotated geometry" of the H-cluster.[10] A chain of water molecules connects protein surface and [4Fe-4S] cluster while conserved amino acids and a small water cluster have been shown to form a dedicated proton transfer trajectory to the diiron site.[11] The protein-cofactor interface is formed by an adjacent cysteine residue and the unique aminodithiolate group (ADT) of the H-cluster (Fig. 1).[12] Any variation of the cysteine or nitrogen head group severely diminishes H_2 turnover, which revealed the essential role of the ADT group as a proton transfer relay.[13–15]

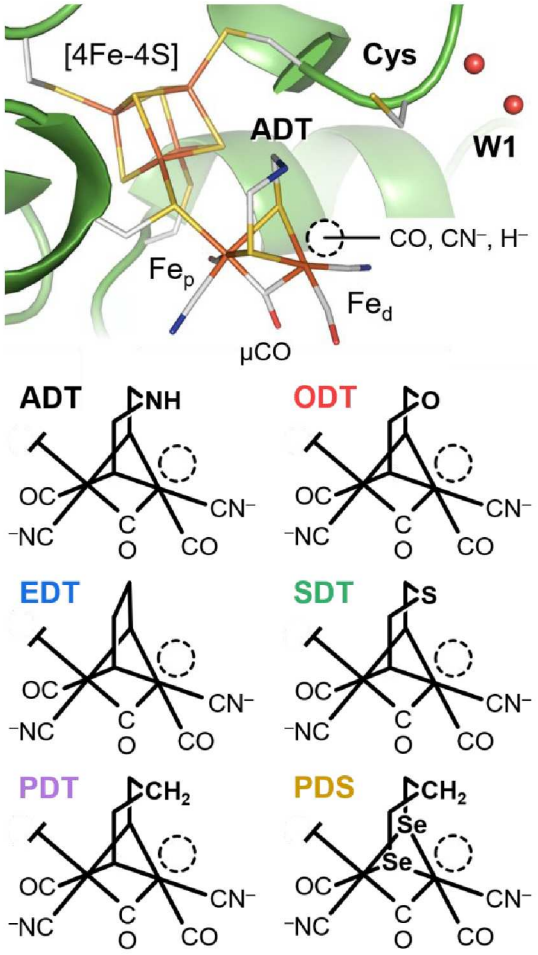

Figure 1. Active site and catalytic cofactor of [FeFe]-hydrogenase. The upper panel shows the active-ready, oxidized H-cluster and the immediate protein environment (pdb entry 4XDC). The catalytic proton transfer pathway includes the aminodithiolate group (ADT), a cysteine (C169 in HYDA1) and a water cluster (W1). The open coordination site (dashed circle) may accommodate CO, CN^-, or H^- ligands. Below, the six analyzed cofactor variants are shown in a simplified representation. Cofactor variant EDT was crystallized here for the first time (pdb entry 6H63).

Various redox states of the H-cluster have been identified (Table 1). For example, proton-coupled electron transfer to the [4Fe-4S] cluster preserves the rotated, Hox-like geometry in the one-electron reduced state **Hred′**.[16–18] Vibrational coupling of ligands in the CO-inhibited

states **Hox-CO** and **Hred´-CO** suggests an additional, equatorial CO ligand and an *apical* cyanide ligand (*a*CN^-) at Fe_d[19] although earlier crystal structures were modeled with an *apical* carbonyl (*a*CO).[20,21] Based on isotope editing studies we proposed *a*CO ligation at the reduced diiron site of **Hred** and **Hsred** together with a *bridging* hydride (μH^-).[22] Other authors favor an open coordination site at Fe_d and a μCO or "semi-bridging" carbonyl ligand in these states.[23–26] In the two-electron reduced catalytic intermediate **Hhyd**, an *apical* hydride species at Fe_d was verified.[27–29] The remarkable flexibility of the diiron site is broadly accepted; however, the molecular proceedings of hydrogen turnover are under debate.[30] How variations in H-cluster geometry are related to hydrogen bonding changes and proton transfer is in the focus of the present investigation.

Table 1. Electronic and structural features of H-cluster species.

redox species	[4Fe-4S] cluster	diiron site†	*bridging* species‡	*apical* species#	alternative annotation	reference
Hox	+2	I / II	CO	*none*	*none*	5,9
Hox-CO	+2	I / II	CO	CN^-	*none*	19
Hred´	+1	I / II	CO	*none*	Hred	16–18
Hred´-CO	+1	I / II	CO	CN^-	Hred-CO	13
Hhyd	+1	II / II	CO	H^-	*none*	27–29
Hred	+2	II / II	H^-	CO	$HredH^+$	22
Hsred	+1	II / II	H^-	CO	$HsredH^+$	22

† Formal redox levels are given for Fe_p / Fe_d.
‡ Alternative *bridging* and *apical* ligands were proposed for **Hred** and **Hsred**.[24–26]
# The crystal structures of CO-inhibited CPI was modeled with an *apical* CO ligand.[20]

In vitro maturation of [FeFe]-hydrogenases generated H-cluster variants that contain artificial dithiolate ligands (Fig. 1) affecting the geometry of the Fe_d site, the reactivity with small molecules, and the hydrogen bonding network at the active site.[31–33] Such cofactor variants show characteristic infrared signatures, accumulate different H-cluster states in the presence of

H_2, and exhibit distinct CO sensitivities.[13–15] These observations prompted us to investigate the underlying substrate affinities and cofactor geometries. Nine variants of the [FeFe]-hydrogenase from *Chlamydomonas reinhardtii* (HYDA1) were compared, including different dithiolate head groups as well as replacements of an adjacent cysteine (C169 in HYDA1) by side-directed mutagenesis. We employed qualitative and quantitative infrared spectroscopy to analyze the reactions with H_2 and/or CO as well as X-ray crystallography, quantum chemical calculations, and kinetic simulations to characterize the structure and function of the variants. Inhibition with CO proved to be a valuable tool for probing the active site properties independent of catalytic activity and functional proton transfer. The drastic variations observed in the stabilization of **Hhyd** and **Hox-CO** are attributed to proton transfer and hydrogen-bonding interactions in the inner and outer coordination sphere[34] of the H-cluster. Such effects were found to determine the geometry of the active site cofactor under catalytic and inhibitory conditions.

RESULTS AND DISCUSSION

[FeFe]-hydrogenase apo-protein from *C. reinhardtii* (HYDA1) was heterologously expressed and synthesized in *E. coli*. After purification, protein was activated with synthetic diiron complexes as described previously.[32] The resulting enzymes were analyzed by *in situ* attenuated total reflection Fourier-transform infrared spectroscopy (ATR FTIR) with regard to reactions with H_2 and CO. The study included native enzyme (ADT) as well as cofactor variants ODT, EDT, and SDT as well as PDT and PDS (Table 2). Furthermore, we addressed protein/ cofactor interactions by comparison of native enzyme with amino acid variant C169A and its cofactor "double" variants ODT and EDT (Table 2). Solving the crystal structure of the EDT variant of [FeFe]-hydrogenase CPI from *Clostridium pasteurianum* verified the lack of a central atom in

the dithiolate bridgehead as well as the absence of a putative water molecule in the respective position. (PDB entry 6H63, Fig. S1).

Table 2. Cofactor and amino acid variants analyzed in this study.

annotation	full name†	head group	position 169‡	additional references
ADT	amino-dt	NH	-CH_2-SH	8,12
ODT	oxo-dt	O	-CH_2-SH	8,14
EDT	ethane-dt	*none*	-CH_2-SH	18
SDT	sulfur-dt	S	-CH_2-SH	8,14
PDT	propane-dt	CH_2	-CH_2-SH	8,13
PDS	propane-ds	CH_2	-CH_2-SH	33
ADT-C169A	amino-dt	NH	-CH_3	*none*
ODT-C169A	oxo-dt	O	-CH_3	*none*
EDT-C169A	ethane-dt	*none*	-CH_3	*none*

† "dt" and "ds" refers to dithiolate and diselenide, respectively

‡ HYDA1 numbering (equivalent 299 in CPI)

Spectral Characterization. The HYDA1 cofactor variants in as-isolated form adopted varying mixtures of oxidized, reduced, and CO-inhibited H-cluster species as visible in the FTIR spectra. A unique identification of the vibrational bands of the CO and CN^- ligands in the oxidized states (**Hox**, **Hox-CO**) and oxidized-protonated states (**HoxH**, **HoxH-CO**), as well as in the corresponding one-electron reduced states (**Hred´**, **Hred´-CO**) was accomplished (Fig. S2, Tables S1 and S2). This is of key importance since **Hox**, **HoxH**, and **Hred´** give rise to similar IR signatures and produce different CO-inhibited species.[17–19] We note that a consistent set of IR spectra of these states for all cofactor variants was so far not available.

Despite catalytic activities typically < 1% relative to native HYDA1,[13,14] near-quantitative enrichment of **Hox** was achieved at pH ≥ 8 upon prolonged exposure to N_2 gas (auto-oxidation,

see Fig. S3). In comparison to ADT, the IR bands of **Hox** for HYDA1 EDT, SDT, and PDT variants showed only small CO/CN$^-$ band frequency up-shifts while ODT exhibited slightly larger up-shifts and bands of PDS are shifted to lower frequencies (Fig. 2A and Fig. S4). Quantum chemical calculations at QM/MM and DFT levels accurately reproduced the CO/CN$^-$ stretching frequencies of **Hox** for all variants (Fig. S5). These results provide strong evidence that the overall electronic configuration of the oxidized H-cluster is similar in all variants. The frequency shifts are explained by small variations in electron density distribution, i.e. due to increased electronegativity of the ODT and SDT head groups[14] or an overall increase of electron density in the PDS variant.[33]

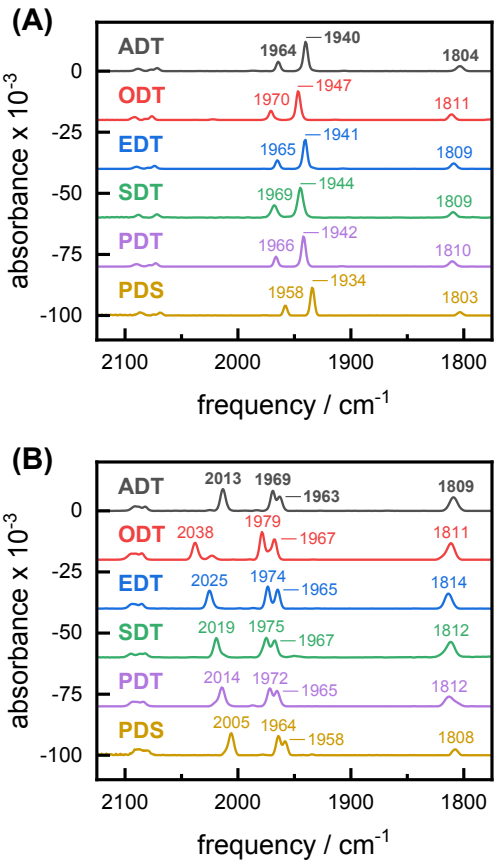

Figure 2. Infrared spectra of HYDA1 cofactor variants. (A) Normalized spectra of **Hox** in the presence of N_2 (pH 8). **(B)** Normalized spectra of **Hox-CO** in the presence of CO (pH 8). See Tables S1 and S2 for CN$^-$ band frequencies.

Exposure of oxidized HYDA1 to CO gas stabilized the CO-inhibited state (Fig. 2B). While the overall IR signature of **Hox-CO** was conserved in all cofactor variants, ODT and EDT showed pronounced up-shifts, in particular of the highest-frequency CO band (25 cm^{-1} or 12 cm^{-1}, respectively). It is important to note that this band results from a coupled vibrational mode involving all CO ligands and must not be assigned to exogenous CO.[19] The mean differences in CN^- stretching frequencies for **Hox-CO** ODT and EDT are the same as in **Hox** (Fig. S4).

Quantum chemistry was employed to evaluate conceivable diiron site geometries for **Hox-CO** (Fig. S5 and S6). Best agreement between experimental and calculated IR frequencies was found for a structure with an *apical* CN^- ligand compared to a geometry with an *apical* CO ligand at Fe_d, as reported earlier.[19] The IR signatures indicate a comparable electronic configuration of the **Hox-CO** cofactor in all variants, in accordance with the data for **Hox**. However, the calculations did not fully reproduce the CO frequency up-shifts as observed for ODT and EDT. This suggests an influence on the electronic configuration of the H-cluster beyond inner coordination sphere effects that could not be included in the calculations. We assume that altered interactions between the H-cluster and its protein environment[35–37] may cause the diverging IR signatures of **Hox-CO** in cofactor variants ODT and EDT, which remain unspecified in the absence of respective crystal structures. In the next step, we explored the influence of the dithiolate group on CO inhibition in kinetic experiments.

Inhibition and Reactivation Kinetics with CO. *In situ* ATR FTIR spectroscopy facilitated a quantitative comparison of CO inhibition and reactivation kinetics for all HYDA1 cofactor variants (Fig. 3). Already at 1% CO partial pressure, ADT, ODT, EDT, and PDS rapidly and completely converted from **Hox** → **Hox-CO**, which indicates similar and high CO binding affinities. In contrast, SDT and PDT adopted only approximately 65% or 20% **Hox-CO** after

250 s under 1% CO (t_1 in Fig. 3) and converted to **Hox-CO** at 100% CO partial pressure only incompletely (~90% or ~70%, respectively). This behavior implied diminished CO binding affinities. Notably, the CO sensitivity of the selenium-substituted PDS variant was similar to ADT, which suggests that changes in charge density distribution and/or conformational flexibility contributes to the apparent CO affinity.[15] Under the chosen conditions, the kinetics of CO inhibition and reactivation were found to be reproducible with an experimental variance not exceeding 5% (Fig. S7, Tab. S4). To investigate CO binding free from macroscopic effects (i.e. gas diffusion) we exploited transient IR spectroscopy in a flash-photolysis approach similar to what was reported by Mirmohades and coworkers.[38,39] Following CO photolysis induced by a 450 nm laser pulse, equally rapid CO re-binding ($t_{1/2}$ = 1.3 ± 0.2 ms) was observed for ADT, ODT, and EDT (Fig. S8). Accordingly, the microscopic velocity of CO binding is independent of the dithiolate head group.

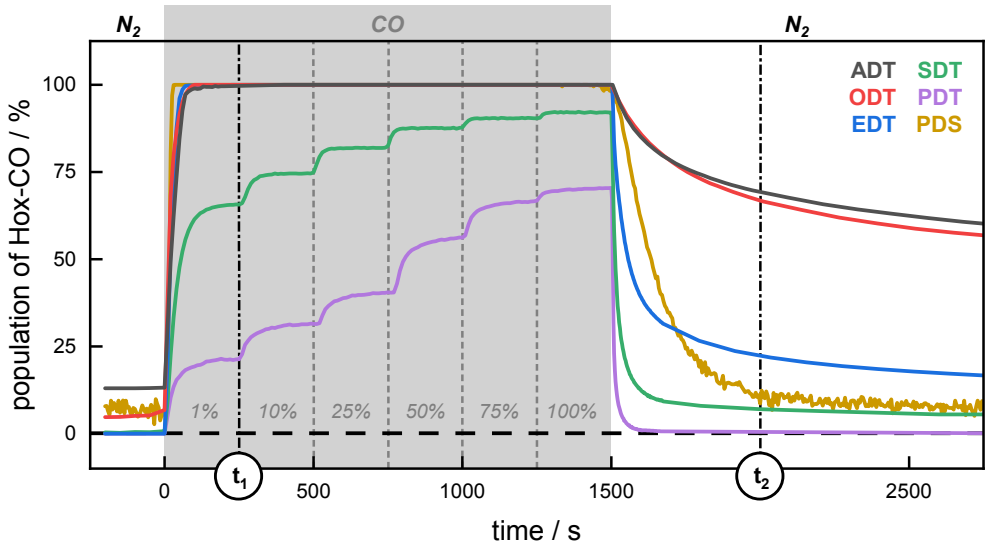

Figure 3. CO inhibition and reactivation kinetics. Relative population of **Hox-CO** (%) as a function of time and CO concentration in the gas phase (0 – 100%). t_1: [**Hox-CO**] after 250 s at 1% CO in 99% N_2. t_2: [**Hox-CO**] at 500 s after removal of CO from the gas stream. ADT, ODT, EDT, and PDS exhibit very similar inhibition kinetics ($t_{1/2}$ < 10 s for 1% CO and full

inhibition after ~60 s). The low CO affinity of SDT and PDT is mirrored in the fast reactivation kinetics; ADT and ODT showed very slow reactivation, accordingly. Despite being easily inhibited by CO, EDT and PDS exhibited relatively fast reactivation.

The varying degrees of CO inhibition were mostly mirrored by the **Hox-CO → Hox** reactivation kinetics in the absence of CO gas (t > 1500 s in Fig. 3). While rapid and almost complete **Hox-CO** decay was observed for SDT and PDT, a slower and incomplete reactivation within the experimental data acquisition period was observed for EDT and PDS. ADT and ODT showed similar but very slow and least complete **Hox-CO** decay. The altered CO inhibition and reactivation kinetics in some of the dithiolate variants suggests that the macroscopic CO affinity is defined by variations of the relative CO binding and release rates and an altered ligand rearrangement, possibly. As a prerequisite for CO binding, earlier studies from our groups[19] have suggested an alternative to the crystalized **Hox** geometry, which is characterized by a partial rotation of the equatorial CN^- ligand at Fe_d. In this structure, the distance between CN^- and ADT-NH is diminished by ~1.3 Å reflecting a weak inner-sphere hydrogen bond in "Hox_b" that may compensate for the proposed outer-sphere hydrogen bond to a lysine residue in the crystallographic conformation of "Hox_a" (Fig. 4A).[35] A similar structural equilibrium of **Hox** has been discussed in the context of O_2 induced deactivation by Fourmond and co-workers.[40] To gain further insight into the observed inhibition and reactivation profiles, we employed numerical simulations including a two-step reaction model with a reversible geometry change (conformational isomers "Hox_a" and "Hox_b"), followed by CO binding to "Hox_b" and formation of **Hox-CO** (Eq. S3, Fig. S9). Variation of the relative rate constants qualitatively reproduced the experimentally observed **Hox-CO** equilibrium populations and rate constants of the dithiolate variants (Fig. 4B).

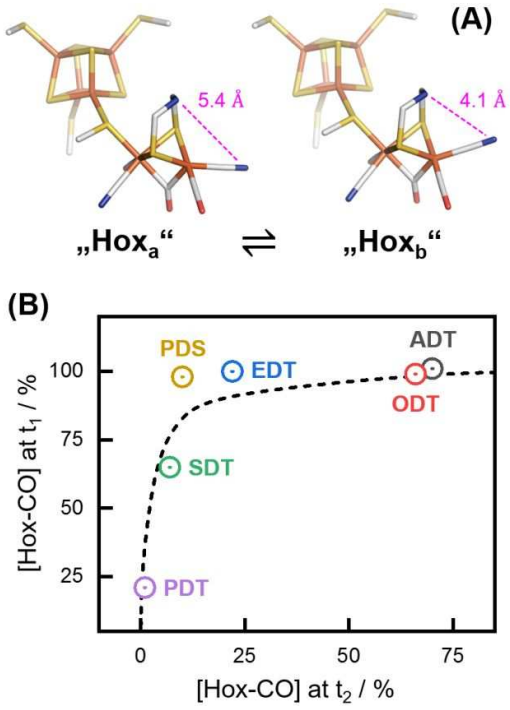

Figure 4. Conceivable isomers of Hox and simulation of relative Hox-CO populations. (A) Out of two structural isomers of the active-ready oxidized state, "Hox$_a$" represents the crystallized geometry while "Hox$_b$" is characterized by a partly rotated, *distal* CN^- ligand. **(B)** Plotting data from Fig. 3 for [**Hox-CO**] at t_1 (inhibition) against [**Hox-CO**] at t_2 (reactivation) illustrates that ADT and ODT have a high CO affinity whereas PDT is relatively CO insensitive. Cofactor variants occupying the upper left of the graph show mixed characteristics. A two-step reaction model with a reversible geometry change followed by CO binding reasonably reproduces the observed behavior (dashed line, see Fig. S9 and the legend for computational details and underlying rate constants that yielded the theoretical **Hox-CO** concentration values).

We suggest that oscillations of the **Hox** geometry determine the apparent **Hox-CO** population and assign the effects of dithiolate exchange to a gradual de-stabilization of a **Hox** isomer with slight ligand rearrangements at Fe_d ("Hox$_b$"). This view is supported by the relative energies of the two **Hox** conformers as derived from DFT calculations, which suggest considerable stabilization of the crystallographic conformation (Hox$_a$) in **Hox**, but stabilization of the

conformation with an *apical* CN^- (*a*CN^-) at Fe_d in **Hox-CO**, as well as destabilization of the *a*CN^- conformation of **Hox-CO** in the non-ADT cofactor variants (see caption of Fig. S9 for details). While simulating absolute rates of CO inhibition and reactivation is not possible at this stage, we aimed at a qualitative description of the kinetic differences between cofactor variants. More complex kinetic models are certainly conceivable, but cannot be uniquely designed at present due to the lack of information on protein-cofactor interactions and other kinetic processes. The observed differences in CO inhibition and reactivation are hardly compatible with an *apical* CO ligand. Weakening of **Hox-CO** thus is attributed to the lack of hydrogen bonding between the dithiolate head group and an *apical* CN^- ligand. However, the reactivation kinetics indicate a higher degree of complexity. This possibly includes electrostatic attraction (ODT, SDT)[14], steric repulsion between the *apical* ligand and the dithiolate head group (PDT)[15], as well as differences in electron density distribution across the diiron site (PDS).[33] A notable spectroscopic feature is the lack of larger changes in the CN^- frequencies among the CO-inhibited cofactor variants (Fig. S2 and Table S2). Previously, the deletion of a putative hydrogen bond donor to Fe_p-CN^- shifted the corresponding IR bands by ~20 cm^{-1} to lower frequencies.[36] Whether outer-sphere hydrogen bonding (i.e. to adjacent amino acid residues or water molecules) may compensate for inner-sphere hydrogen bonding in cofactor variants ODT and EDT was probed in the next step.

Outer-sphere stabilization of Hox-CO. Cysteine 169 functions as a proton relay between the H-cluster and water cluster W1. It represents a likely hydrogen-bond donor in the vicinity of the H-cluster. To probe the influence of C169 on CO affinity, we produced site-directed mutagenesis variants with a cysteine/ alanine exchange. HYDA1-C169A was reconstituted with ADT, ODT, or EDT cofactors and analyzed by *in situ* ATR FTIR spectroscopy (Fig. 5 and Fig. S10). In comparison to wild-type enzyme, the spectra of **Hox** exhibited a mean CO/CN^- down-shift of only ~3 cm^{-1} whereas the **Hox-CO** signature of the HYDA1-C169A cofactor variants

indicated much stronger shifts to lower frequencies. For example, the coupled CO modes β and δ shift by 8 – 12 cm^{-1} and 24 – 28 cm^{-1}, respectively. Band γ that comprises significant contributions from the proximal CO ligand did not change significantly. The difference spectra for ADT, ODT, and EDT in Figure 5 show that the **Hox-CO** signature of HYDA1-C169A is not the same; however, the dithiolate-specific IR band up-shifts observed in CO-inhibited wild-type enzyme (Fig. 2B) were found to be largely remedied. The **Hox-CO** spectrum of HYDA1-C169A ADT was hardly affected by the amino acid exchange.

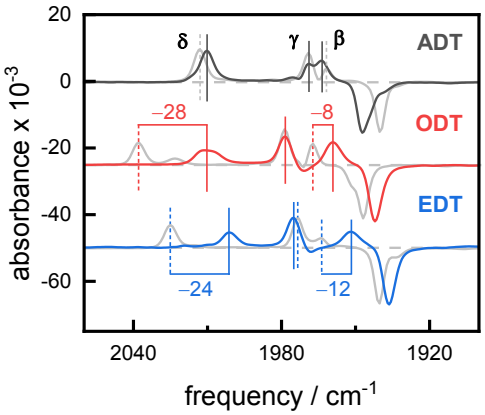

Figure 5. ATR FTIR difference spectra of the Hox → Hox-CO conversion. Spectra of the C169A variant of HYDA1 are shown as colored lines, grey spectra depict wild-type enzyme. The frequencies of the CO vibrational modes of **Hox-CO** (positive bands β, γ, and δ) are sensitive to the H-clusters' geometry. Negative bands are assigned to **Hox**. Significant downshifts are indicated in cm^{-1} (IR bands β and δ, predominantly). Only limited differences in **Hox-CO** were observed between native HYDA1 and HYDA1-C169 (ADT).

We recently solved the crystal structure of CPI-C299A in oxidized form (equivalent to HYDA1-C169A).[11] Here, the cysteine is replaced by a water molecule, W* (Fig. S11). Although CPI-C299A was not crystalized in CO-inhibited form, no variation of internal water was observed upon CO inhibition of native enzyme[20,21] suggesting conserved localization of W* in both **Hox** and **Hox-CO**. This water species may act as a hydrogen bond donor to the

apical CN^- ligand of **Hox-CO** when inner-sphere hydrogen bonding is impeded (i.e., in ODT and EDT). The similar IR signatures of the CO-inhibited C169A variants (Fig. 5) suggest an unconstrained ligand orientation reflecting the structural flexibility of the water molecule acting as a hydrogen bond donor. Furthermore, hydrogen bonding to W* (instead of C169) may explain the lack of significant differences in the CN^- regime "rescuing" the native **Hox-CO** signature. We conclude that the hydrogen-bonding network between polar, *apical* ligands at the H-cluster and the adjacent cysteine sidechain or neighboring water species is an important determinant of the diiron site geometry in the non-ADT variants.

Hydrogen Oxidation Kinetics. To investigate the geometry of the H-cluster in reduced form, we explored the reaction with H_2 of different HYDA1 cofactor variants by *in situ* ATR FTIR spectroscopy (Fig. 6). In the presence of H_2, native ADT enzyme revealed a complex mixture of **Hred´** and **Hred/Hsred** at pH 8 (top left) while near-quantitative **Hhyd** formation was observed at pH 4 (top right).[29] Independent of the pH, cofactor variants PDT and PDS formed no other redox species than **Hred´** whereas SDT enzyme did not react with H_2 at all (Fig. S12).[14,15] ODT and EDT revealed a large population of **Hred´** and **Hhyd** already at pH 8.[28] The EDT-modified enzyme showed an immediate **Hox** → **Hred´** conversion followed by progressive enrichment of **Hhyd** over **Hred´** (bottom left). These processes occur simultaneously in HYDA1-ODT (bottom right). For subsequent replacement of H_2 with N_2, native enzyme exhibited the slowest **Hhyd** decrease, HYDA1-EDT the fastest decrease, and cofactor variant ODT adopted medium-speed decay kinetics (Fig. S13). Notably, **Hred** and **Hsred** were exclusively observed in HYDA1-ADT, which illustrates the need for efficient proton transfer in the reduction of the diiron site.

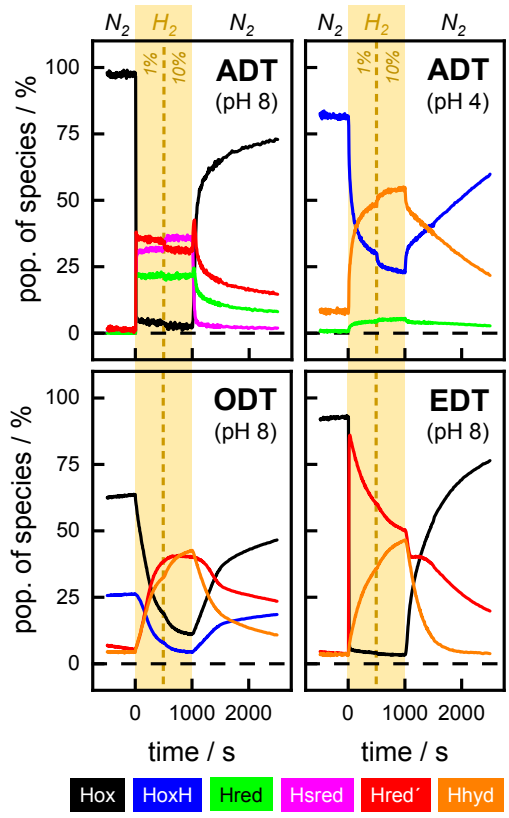

Figure 6. H_2 oxidation kinetics. Changes of H-cluster populations in HYDA1 enzyme in the presence of 0%, 1%, or 10% H_2 in the N_2 carrier gas. **Top left:** In native enzyme, exposure to H_2 caused an immediate accumulation of reduced cofactor states **Hred**/ **Hsred** and **Hred´** at the expense of **Hox** (pH 8). When H_2 was removed from the gas phase, a short-lived increase of **Hred** and **Hred´** at the expense of **Hsred** was observed. **Top right:** At pH 4, native enzyme predominantly formed **Hhyd** and traces of **Hred** out of **HoxH**. **Bottom left:** Cofactor variant ODT was found to accumulate **Hred´** and **Hhyd** slowly and simultaneously. Even at pH 8, the oxidized sample comprised ~25 % **HoxH**. **Bottom right:** Cofactor variant EDT reacts much faster with H_2 than ODT, first converting from **Hox** to **Hred´** and thereafter from **Hred´** to **Hhyd** (pH 8). Both ODT and EDT show no traces of **Hred**/ **Hsred**. The persistence of **Hhyd** in the absence of H_2 decreases in the following order: ADT > ODT > EDT.

The H-cluster binds an *apical* hydride ligand (*a*H$^-$) at the *distal* iron ion in **Hhyd**.[27–29] It seems reasonable to assume hydrogen bonding between *a*H$^-$ and ADT-NH stabilizing the charged *apical* ligand, similar to the situation in **Hox-CO** (see above). However, to understand the formation and stabilization of **Hhyd** in cofactor variants ODT and EDT, both thermodynamic and kinetic considerations must be taken into account. High proton concentrations[11,29] or partly impaired proton transfer activity[27,28] to the diiron site have been exploited to accumulate **Hhyd** in functional enzyme. Hydride formation in ODT and EDT is facilitated by outer-sphere stabilization between *a*H$^-$ and the protein environment, most likely compensating for the lack of an inner-sphere hydrogen bond donor (i.e., ADT-NH). In contrast to HYDA1-C169A, the double variants HYDA1-C169A ODT and EDT were found to be completely unreactive with H_2 (Fig. S12). Revisiting CO inhibition is informative here. The double variants were easily inhibited by CO, explained by the presence of an additional water molecule in HYDA1-C169A, W* (Fig. 5). Although a similar arrangement should be able to stabilize the hydride state, heterolytic cleavage of H_2 was not observed. This illustrates the role of proton transfer in the accumulation of reduced species like **Hhyd** and allows concluding that the geometry of the H-cluster is determined by both hydrogen bonding and proton transfer.

Direct evidence for a similar mechanism of **Hhyd** and **Hox-CO** stabilization was derived from concerted H_2 and CO treatments on HYDA1 (Fig. 7). The top left panel shows the concomitant decrease of **Hred/Hsred** and **Hred´** at 1% or 10% CO in H_2 carrier gas in native enzyme (pH 8). Different to inhibition under oxidizing conditions, CO inhibition in the presence of H_2 yielded a combination of **Hred´-CO** and **Hox-CO**, indicating an incomplete oxidation. Compared to Fig. 3A, native enzyme reacts significantly slower with CO and recovers from inhibition about four times faster under H_2 (Fig. S14). This reflects the higher affinity of CO compared to H_2 of the ADT H-cluster.[41] Furthermore, a small yet significant fraction of **Hred/Hsred** remains to be stable with 1% CO whereas **Hred´** is lost completely under these

conditions (Fig. S15). While **Hred´** is characterized by μCO ligand with an open coordination site at Fe_d,[16–18] reduction of the diiron site apparently provides mild protection against exogenous CO. The ability of native enzyme to accumulate H-cluster intermediates with a reduced diiron site (**Hred/Hsred**) likely contributes to the enhanced reactivation from CO-inhibition in the presence of H_2, which is not observed in HYDA1-ODT (see Fig. S14). It remains to be evaluated if this is due to changes in redox state or caused by conformational changes as suggested earlier.[22]

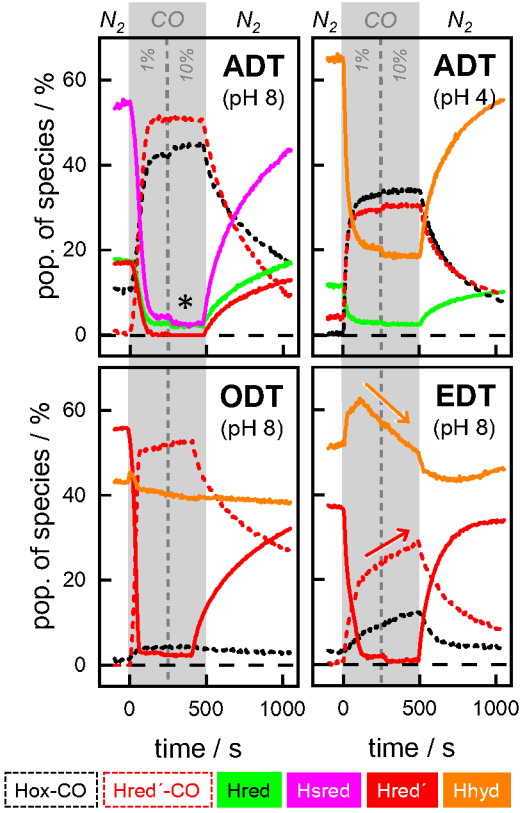

Figure 7. CO inhibition and reactivation in the presence of H_2. Changes of H-cluster populations in HYDA1 enzyme in the presence of 0%, 1%, or 10% H_2 (carrier gas H_2). **Top left:** In native enzyme (pH 8), exposure to CO caused an immediate decrease of reduced cofactor states **Hred**/ **Hsred** and **Hred´**. Asterisks: about 5% **Hred**/ **Hsred** remain stable under 1% CO (see Fig. S15). **Top right:** The hydride state predominantly formed at pH 4 is

diminished to ~20% under CO. **Bottom left:** In cofactor variant ODT an increase of **Hred´-CO** over **Hred´** was observed upon CO exposure (pH 8), but virtually no decrease of **Hhyd**. **Bottom right:** In comparison, slow changes in **Hhyd** in the presence of CO indicate that **Hhyd** in EDT was less stable than in ODT.

Distinct protection against CO was observed when the H-cluster was locked in the hydride state, i.e. at pH 4 (Fig. 7, top right panel). In the presence of 10% CO, approximately >20 % **Hhyd** prevailed. This effect was found to be even more pronounced in the cofactor variants, even at alkaline pH values. For example, HYDA1-ODT showed conversion of **Hred´** to **Hred´-CO** but virtually no decrease of **Hhyd** (bottom left) whereas a very slow conversion of **Hhyd** into CO-inhibited species was notable in HYDA1-EDT (bottom right). The higher stability of the hydride state in cofactor variant ODT vs. EDT agrees well with decrease kinetics of **Hhyd** (Fig. S13) and **Hox-CO** (Fig. 3) as discussed above. Our systematic evaluation of the reactivity of HYDA1 cofactor variants with CO and H_2 emphasizes that inner coordination sphere interactions are a major determinant for stabilization of *apical* ligands in both **Hox-CO** and **Hhyd**.

CONCLUSIONS

Our experimental and computational analysis of the [FeFe]-hydrogenase from *C. reinhardtii* consistently implies that the CO/CN^- ligand dynamics of the H-cluster are governed by proton transfer and hydrogen-bonding interactions at the inner coordination sphere (Fig. 8). We propose an intrinsically flexible diiron site geometry[19,40] that facilitates stabilization of polar ligands at the *distal* iron ion in both catalytic intermediates (**Hhyd**) and inhibited species (**Hox-CO**). Comparing H_2 oxidation and CO inhibition allows dissecting the influence of proton transfer and hydrogen bonding on the geometry of the H-cluster.

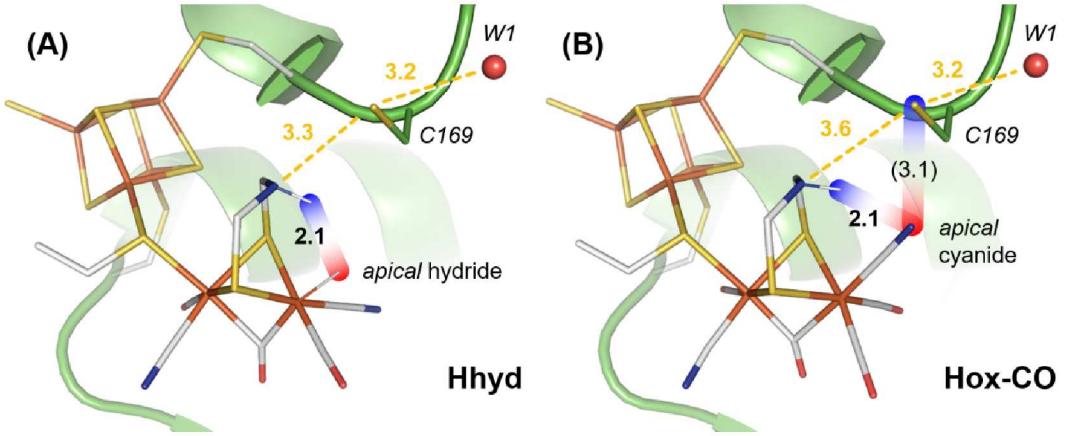

Figure 8. Proton transfer and hydrogen bonding at the H-cluster. DFT models of the H-cluster in the **Hhyd** and **Hox-CO** state were superposed with the crystal structure of CPI (pdb entry 4XDC). Dashed lines suggest potential proton transfer trajectories. Blue and red color indicate positive and negative (partial) charges, respectively. All distances are given in 10 m^{-10} (Å). **(A)** In native enzyme, inner-sphere hydrogen bonding stabilizes the *apical* hydride ligand of **Hhyd**. Variants with no proton transfer activity did not accumulate **Hhyd**. **(B)** The CO-inhibited state **Hox-CO** is stabilized by either inner or outer coordination sphere hydrogen-bonding to the *apical* cyanide ligand, depending on the nature of the dithiolate headgroup. Accumulation of **Hox-CO** is independent of proton transfer.

For the native enzyme, stabilization is mainly achieved by inner-sphere hydrogen bonding between ADT-NH and the *apical* hydride ligand of **Hhyd** or the *apical* cyanide ligand of **Hox-CO**. For cofactor variants with a less polar dithiolate group, stabilization of a particular diiron site geometry is determined by outer coordination sphere interactions, i.e. hydrogen-bonding to adjacent amino acid side chains and/or water species (Fig. 8). Our findings further suggest different H-cluster geometries for **Hox/Hred´** and **Hred/Hsred**, emphasizing the need for combined crystallographic and spectroscopic studies on the reduced or "H_2-inhibited" states of [FeFe]-hydrogenases.[30] Comparative CO inhibition and H_2 oxidation experiments helped identifying such correlations and facilitated a detailed understanding of hydrogen bonding and

proton transfer at the protein-cofactor interface of [FeFe]-hydrogenases. The derived concepts for tuning of proton transfer efficiency and stabilization of catalytic cofactor intermediates in [FeFe]-hydrogenases may inspire synthetic H_2-forming catalysts for the production of H_2 as a fuel.[42–44]

Inner-sphere hydrogen bonding may also play a role in O_2 sensitivity as a putative intermediate of O_2-induced H-cluster degradation, **Hox-O_2**, has been shown to carry an *apical* superoxide ligand.[45] From an evolutionary perspective, it appears that the excellent catalytic performance of [FeFe]-hydrogenases has evolved at the expense of CO and O_2 sensitivity. For [FeFe]-hydrogenases of photosynthetic organisms like *C. reinhardtii*,[46] this may have been an advantage as CO liberated due to transient exposure of the enzymes to O_2 or high light intensities may protect catalytically competent enzymes from deactivation.[47–49]

MATERIAL AND METHODS

Artificial maturation and protein crystallography. [FeFe]-hydrogenase apo-protein from *C. reinhardtii* (HYDA1) and *C. pasteurianum* (CPI) was expressed in in Escherichia coli (BL21(DE3)-ΔiscR) and purified as previously described; cofactor synthesis and in vitro maturation of protein was performed following established protocols.[32,33] Diffraction data on protein crystals of the semisynthetic CPI hydrogenase EDT were collected at 100 K at beamline ESRF-BM30A (Grenoble, France) and processed as reported earlier.[8] The crystal structure was deposited in the Protein Data Bank under accession code 6H63. Crystallographic data is summarized in Table S3. See Supporting Information for further experimental details.

ATR FTIR spectroscopy and data evaluation. Infrared spectra were recorded on protein films using FTIR spectroscopy in attenuated total reflection configuration on a Bruker Tensor27 spectrometer.[18] H-cluster states were populated in the presence of defined compositions of N_2,

CO, or H_2 in a humidified, pH-controlled gas stream ("aerosol"). To monitor the H-cluster state conversions in time, IR spectra were collected in real time with a temporal resolution of 1 - 5 s. Data evaluation involved normalization of spectra followed by a global fit approach in the CO/CN^- regime to determine cofactor state populations.[18] See Supporting Information for further details.

Transient IR spectroscopy. Samples of HYDA1 ADT, ODT, and EDT variants were mixed (3 µL of ~1 mM protein), dehydrated under CO gas on a BaF_2 window, rehydrated via vapor diffusion, and sealed with a second BaF_2 window. Photolysis of the exogenous CO ligand was induced by a 10 ns flash (~ 90 mJ/cm^2, 450 nm) from an optical parametric oscillator pumped by the third harmonic of a Nd:YAG laser (Quanta-Ray). IR transients (2000 – 2045 cm^{-1}, 1 cm^{-1} steps, 100 repetitions at 1 Hz each) were recorded on a homebuilt continuous-wave quantum-cascade laser (QCL) spectrometer.[39] See Supporting Information for further details.

Computational procedures. Density functional theory and quantum mechanics/ molecular mechanics calculations (BP86 or TPSSh functionals and TZVP basis-set, broken-symmetry approach for geometry-optimization and antiferromagnetic couplings calculation, ONIOM method and universal force field in QM/MM) on model structures (Fig. S16) were carried out using Gaussian09 as reported in ref. 50. Vibrational frequencies were derived from normal mode analysis of relaxed structures. Numerical kinetic simulations were performed with the CAIN ordinary differential equation solver (available at http://cain.sourceforge.net). See Supporting Information (computational procedures and references therein, Figs. S5, S6, S8, and S15) for further details.

SUPPORTING INFORMATION

Supporting experimental procedures; Supporting computational procedures; Comparison of ADT and EDT; Comparison of Hox/HoxH and Hox-CO/HoxH-CO; Auto-oxidation in the absence of H2; Experimental CO band frequency differences; Calculation of vibrational frequencies; Reproducibility and variance; Transient IR spectroscopy; Kinetic simulations; Absolute spectra for HYDA1-C169A; Comparison of native CPI and CPI-C299A; Spectra of all cofactor variants in the presence of H_2; Stability of Hhyd in the absence of H_2; Reactivation from CO-inhibition in ADT and ODT; Durability of Hsred in the presence of H_2 and CO; Computational structures; IR-frequencies for H-cluster species with a Hox-like diiron site geometry (table); IR-frequencies for CO-inhibited H-cluster species (table); Data collection and refinement statistics of crystal structure CPI-EDT (table); Fitting parameters (table); XYZ coordinates (table).

ACKNOWLEDGEMENTS

We thank all reviewers for their valuable input. STS acknowledges M.-H. Chiang for inspiring discussions. STS is funded by the DFG within the framework of priority program 1927 (1554/5-1). MH and JH acknowledge financial support within UniSysCat (Cluster of Excellence Berlin). JD, MW, and TH acknowledge financial support from the Volkswagen Stiftung (Az 93412), the RESOLV Cluster of Excellence Bochum (EXC 1069), and the China Scholarship Council. FW and UPA thank the DFG (AP242/2-1), the Fraunhofer Internal Programs (ATTRACT 097-602175), and the Studienstiftung des Deutschen Volkes for financial support. We thank the staff of beamline BM30A at the European Synchrotron Radiation Facility (ESRF) for technical support during data collection.

REFERENCES

(1) Lubitz, W.; Ogata, H.; Ru, O.; Reijerse, E. Hydrogenases. *Chem. Rev.* **2014**, *114* (8), 4081–4148. https://doi.org/10.1021/cr4005814.

(2) Vincent, K. A.; Parkin, A.; Lenz, O.; Albracht, S. P. J.; Fontecilla-Camps, J. C.; Cammack, R.; Friedrich, B.; Armstrong, F. A. Electrochemical Definitions of O2 Sensitivity and Oxidative Inactivation in Hydrogenases. *J. Am. Chem. Soc.* **2005**, *127* (51), 18179–18189. https://doi.org/10.1021/ja055160v.

(3) Stripp, S. T.; Goldet, G.; Brandmayr, C.; Sanganas, O.; Vincent, K. A.; Haumann, M.; Armstrong, F. A.; Happe, T. How Oxygen Attacks [FeFe] Hydrogenases from Photosynthetic Organisms. *Proc. Natl. Acad. Sci. U. S. A.* **2009**, *106* (41), 17331–17336. https://doi.org/10.1073/pnas.0905343106.

(4) De Lacey, A. L.; Stadler, C.; Fernandez, V. M.; Hatchikian, E. C.; Fan, H.-J.; Li, S.; Hall, M. B. IR Spectroelectrochemical Study of the Binding of Carbon Monoxide to the Active Site of Desulfovibrio Fructosovorans Ni-Fe Hydrogenase. *J. Biol. Inorg. Chem.* **2002**, *7* (3), 318–326. https://doi.org/10.1007/s00775-001-0301-7.

(5) Roseboom, W.; De Lacey, A. L.; Fernandez, V. M.; Hatchikian, E. C.; Albracht, S. P. J. The Active Site of the [FeFe]-Hydrogenase from Desulfovibrio Desulfuricans. II. Redox Properties, Light Sensitivity and CO-Ligand Exchange as Observed by Infrared Spectroscopy. *J. Biol. Inorg. Chem.* **2006**, *11* (1), 102–118. https://doi.org/10.1007/s00775-005-0040-2.

(6) Peters, J. W.; Lanzilotta, W. N.; Lemon, B. J.; Seefeldt, L. C. X-Ray Crystal Structure of the Fe-Only Hydrogenase (CpI) from Clostridium Pasteurianum to 1.8 Angstrom Resolution. *Science* **1998**, *282* (5395), 1853–1858. https://doi.org/10.1126/science.282.5395.1853.

(7) Nicolet, Y.; Piras, C.; Legrand, P.; Hatchikian, C. E.; Fontecilla-Camps, J. C. Desulfovibrio Desulfuricans Iron Hydrogenase: The Structure Shows Unusual Coordination to an Active Site Fe Binuclear Center. *Structure* **1999**, *7* (1), 13–23. https://doi.org/10.1016/S0969-2126(99)80005-7.

(8) Esselborn, J.; Muraki, N.; Klein, K.; Engelbrecht, V.; Metzler-Nolte, N.; Apfel, U.-P.; Hofmann, E.; Kurisu, G.; Happe, T. A Structural View of Synthetic Cofactor Integration into [FeFe]-Hydrogenases. *Chem. Sci.* **2016**, *7*, 959–968. https://doi.org/10.1039/C5SC03397G.

(9) Silakov, A.; Reijerse, E. J.; Albracht, S. P. J.; Hatchikian, E. C.; Lubitz, W. The Electronic Structure of the H-Cluster in the [FeFe]-Hydrogenase from Desulfovibrio Desulfuricans: A Q-Band 57Fe-ENDOR and HYSCORE Study. *J. Am. Chem. Soc.* **2007**, *129* (37), 11447–11458. https://doi.org/10.1021/ja072592s.

(10) Singleton, M. L.; Bhuvanesh, N.; Reibenspies, J. H.; Darensbourg, M. Y. Synthetic Support of De Novo Design: Sterically Bulky [FeFe]-Hydrogenase Models. *Angew. Chemie Int. Ed.* **2008**, *47* (49), 9492–9495. https://doi.org/10.1002/anie.200803939.

(11) Duan, J.; Senger, M.; Esselborn, J.; Engelbrecht, V.; Wittkamp, F.; Apfel, U.-P.; Hofmann, E.; Stripp, S. T.; Happe, T.; Winkler, M. Crystallographic and Spectroscopic Assignment of the Proton Transfer Pathway in [FeFe]-Hydrogenases. *Nat. Commun.* **2018**, *9*, 4726. https://doi.org/10.1038/s41467-018-07140-x.

(12) Silakov, A.; Wenk, B.; Reijerse, E.; Lubitz, W. 14N HYSCORE Investigation of the H-Cluster of [FeFe] Hydrogenase: Evidence for a Nitrogen in the Dithiol Bridge. *Phys. Chem. Chem. Phys.* **2009**, *11* (31), 6553–6554. https://doi.org/10.1039/b913085n.

(13) Adamska-Venkatesh, A.; Krawietz, D.; Siebel, J. F.; Weber, K.; Happe, T.; Reijerse, E.; Lubitz, W. New Redox States Observed in [FeFe] Hydrogenases Reveal Redox Coupling within the H-Cluster. *J. Am. Chem. Soc.* **2014**, *136* (32), 11339–11346. https://doi.org/10.1021/ja503390c.

(14) Siebel, J. F.; Adamska-Venkatesh, A.; Weber, K.; Rumpel, S.; Reijerse, E.; Lubitz, W. Hybrid [FeFe]-Hydrogenases with Modified Active Sites Show Remarkable Residual Enzymatic Activity. *Biochemistry* **2015**, *54* (7), 1474–1483. https://doi.org/10.1021/bi501391d.

(15) Sommer, C.; Rumpel, S.; Roy, S.; Farès, C.; Artero, V.; Fontecave, M.; Reijerse, E.; Lubitz, W. Spectroscopic Investigations of a Semi-Synthetic [FeFe] Hydrogenase with Propane Di-Selenol as Bridging Ligand in the Binuclear Subsite: Comparison to the Wild Type and Propane Di-Thiol Variants. *J. Biol. Inorg. Chem.* **2018**, *23* (3), 481–491. https://doi.org/10.1007/s00775-018-1558-4.

(16) Katz, S.; Noth, J.; Horch, M.; Shafaat, H. S.; Happe, T.; Hildebrandt, P.; Zebger, I. Vibrational Spectroscopy Reveals the Initial Steps of Biological Hydrogen Evolution. *Chem. Sci.* **2016**, *7*, 6746–6752. https://doi.org/10.1039/C6SC01098A.

(17) Senger, M.; Laun, K.; Wittkamp, F.; Duan, J.; Haumann, M.; Happe, T.; Winkler, M.; Apfel, U.-P.; Stripp, S. T. Proton-Coupled Reduction of the Catalytic [4Fe-4S] Cluster in [FeFe]-Hydrogenases. *Angew. Chemie Int. Ed.* **2017**, *56* (52), 16503–16506. https://doi.org/10.1002/anie.201709910.

(18) Senger, M.; Mebs, S.; Duan, J.; Shulenina, O.; Laun, K.; Kertess, L.; Wittkamp, F.; Apfel, U.-P.; Happe, T.; Winkler, M.; et al. Protonation/Reduction Dynamics at the [4Fe–4S] Cluster of the Hydrogen-Forming Cofactor in [FeFe]-Hydrogenases. *Phys. Chem. Chem. Phys.* **2018**, *20*, 3128–3140. https://doi.org/10.1039/C7CP04757F.

(19) Senger, M.; Mebs, S.; Duan, J.; Wittkamp, F.; Apfel, U.-P.; Heberle, J.; Haumann, M.; Stripp, S. T. Stepwise Isotope Editing of [FeFe]-Hydrogenases Exposes Cofactor Dynamics. *Proc. Natl. Acad. Sci. U. S. A.* **2016**, *113* (30), 8454–8459. https://doi.org/10.1073/pnas.1606178113.

(20) Lemon, B. J.; Peters, J. W. Binding of Exogenously Added Carbon Monoxide at the Active Site of the Iron-Only Hydrogenase (CpI) from Clostridium Pasteurianum. *Biochemistry* **1999**, *38* (40), 12969–12973. https://doi.org/10.1021/bi9913193.

(21) Lemon, B. J.; Peters, J. W. Photochemistry at the Active Site of the Carbon Monoxide Inhibited Form of the Iron-Only Hydrogenase (CpI). *J. Am. Chem. Soc.* **2000**, *122* (15), 3793–3794. https://doi.org/10.1021/ja9943703.

(22) Mebs, S.; Senger, M.; Duan, J.; Wittkamp, F.; Apfel, U.-P.; Happe, T.; Winkler, M.; Stripp, S. T.; Haumann, M. Bridging Hydride at Reduced H-Cluster Species in [FeFe]-Hydrogenases Revealed by Infrared Spectroscopy, Isotope Editing, and Quantum Chemistry. *J. Am. Chem. Soc.* **2017**, *139* (35), 12157–12160. https://doi.org/10.1021/jacs.7b07548.

(23) Nicolet, Y.; De Lacey, A. L.; Vernède, X.; Fernandez, V. M.; Hatchikian, E. C.; Fontecilla-Camps, J. C. Crystallographic and FTIR Spectroscopic Evidence of Changes

in Fe Coordination upon Reduction of the Active Site of the Fe-Only Hydrogenase from Desulfovibrio Desulfuricans. *J. Am. Chem. Soc.* **2001**, *123* (8), 1596–1601. https://doi.org/10.1021/ja0020963.

(24) Adamska-Venkatesh, A.; Silakov, A.; Lambertz, C.; Rüdiger, O.; Happe, T.; Reijerse, E.; Lubitz, W. Identification and Characterization of the "Super-Reduced" State of the H-Cluster in [FeFe] Hydrogenase: A New Building Block for the Catalytic Cycle? *Angew. Chemie Int. Ed.* **2012**, *51* (46), 11458–11462. https://doi.org/10.1002/anie.201204800.

(25) Sommer, C.; Adamska-Venkatesh, A.; Pawlak, K.; Birrell, J. A.; Rüdiger, O.; Reijerse, E. J.; Lubitz, W. Proton Coupled Electronic Rearrangement within the H-Cluster as an Essential Step in the Catalytic Cycle of [FeFe] Hydrogenases. *J. Am. Chem. Soc.* **2017**, *139* (4), 1440−1443. https://doi.org/10.1021/jacs.6b12636.

(26) Ratzloff, M. W.; Artz, J. H.; Mulder, D. W.; Collins, R. T.; Furtak, T. E.; King, P. W. CO-Bridged H-Cluster Intermediates in the Catalytic Mechanism of [FeFe]-Hydrogenase CaI. *J. Am. Chem. Soc.* **2018**, *140* (24), 7623–7628. https://doi.org/10.1021/jacs.8b03072.

(27) Mulder, D. W.; Guo, Y.; Ratzloff, M. W.; King, P. W. Identification of a Catalytic Iron-Hydride at the H-Cluster of [FeFe]-Hydrogenase. *J. Am. Chem. Soc.* **2016**, *139* (1), 83–86. https://doi.org/10.1021/jacs.6b11409.

(28) Reijerse, E. J.; Pham, C. C.; Pelmenschikov, V.; Gilbert-wilson, R.; Adamska-Venkatesh, A.; Siebel, J. F.; Gee, L. B.; Yoda, Y.; Tamasaku, K.; Lubitz, W.; et al. Direct Observation of an Iron-Bound Terminal Hydride in [FeFe]- Hydrogenase by Nuclear Resonance Vibrational Spectroscopy. *J. Am. Chem. Soc.* **2017**, *139* (12), 4306–4309. https://doi.org/10.1021/jacs.7b00686.

(29) Winkler, M.; Senger, M.; Duan, J.; Esselborn, J.; Wittkamp, F.; Hofmann, E.; Apfel, U.-P.; Stripp, S. T.; Happe, T. Accumulating the Hydride State in the Catalytic Cycle of [FeFe]-Hydrogenases. *Nat. commun.* **2017**, *8* (16115), 1–7. https://doi.org/10.1038/ncomms16115.

(30) Haumann, M.; Stripp, S. T. The Molecular Proceedings of Biological Hydrogen Turnover. *Acc. Chem. Res.* **2018**, *51* (8), 1755–1763. https://doi.org/10.1021/acs.accounts.8b00109.

(31) Berggren, G.; Adamska-Venkatesh, A.; Lambertz, C.; Simmons, T. R.; Esselborn, J.; Atta, M.; Gambarelli, S.; Mouesca, J.-M.; Reijerse, E. J.; Lubitz, W.; et al. Biomimetic Assembly and Activation of [FeFe]-Hydrogenases. *Nature* **2013**, *499* (7456), 66–69. https://doi.org/10.1038/nature12239.

(32) Esselborn, J.; Lambertz, C.; Adamska-Venkatesh, A.; Simmons, T.; Berggren, G.; Noth, J.; Siebel, J. F.; Hemschemeier, A.; Artero, V.; Reijerse, E.; et al. Spontaneous Activation of [FeFe]-Hydrogenases by an Inorganic [2Fe] Active Site Mimic. *Nat. Chem. Biol.* **2013**, *9*, 607–609. https://doi.org/10.1038/nchembio.1311.

(33) Kertess, L.; Wittkamp, F.; Sommer, C.; Esselborn, J.; Rüdiger, O.; Reijerse, E.; Hofmann, E.; Lubitz, W.; Winkler, M.; Happe, T.; et al. Chalcogenide Substitution in the [2Fe]-Cluster of [FeFe]-Hydrogenases Conserves High Enzymatic Activity. *Dalt. Trans.* **2017**, *46*, 16947–16958. https://doi.org/10.1039/C7DT03785F.

(34) Ginovska-Pangovska, B.; Dutta, A.; Reback, M. L.; Linehan, J. C.; Shaw, W. J.

Beyond the Active Site: The Impact of the Outer Coordination Sphere on Electrocatalysts for Hydrogen Production and Oxidation. *Acc. Chem. Res.* **2014**, *47* (8), 2621–2630. https://doi.org/10.1021/ar5001742.

(35) Knörzer, P.; Silakov, A.; Foster, C. E.; Armstrong, F. A.; Lubitz, W.; Happe, T. Importance of the Protein Framework for Catalytic Activity of [FeFe]-Hydrogenases. *J. Biol. Chem.* **2012**, *287* (2), 1489–1499. https://doi.org/10.1074/jbc.M111.305797.

(36) Lampret, O.; Adamska-Venkatesh, A.; Konegger, H.; Wittkamp, F.; Apfel, U.-P.; Reijerse, E. J.; Lubitz, W.; Rü, O.; Happe, T.; Winkler, M. Interplay between CN Ligands and the Secondary Coordination Sphere of the H-Cluster in [FeFe]-Hydrogenases. *J. Am. Chem. Soc.* **2017**, *139* (50), 18222–18230. https://doi.org/10.1021/jacs.7b08735.

(37) Pham, C. C.; Mulder, D. W.; Pelmenschikov, V.; King, P. W.; Ratzloff, M. W.; Wang, H.; Mishra, N.; Alp, E. E.; Zhao, J.; Hu, M. Y.; et al. Terminal Hydride Species in [FeFe]-Hydrogenases Are Vibrationally Coupled to the Active Site Environment. *Angew. Chemie Int. Ed.* **2018**, *57* (33), 10605–10609. https://doi.org/10.1002/anie.201805144.

(38) Mirmohades, M.; Adamska-Venkatesh, A.; Sommer, C.; Reijerse, E.; Lomoth, R.; Lubitz, W.; Hammarström, L. Following [FeFe] Hydrogenase Active Site Intermediates by Time- Resolved Mid-IR Spectroscopy. *J. Phys. Chem. Lett.* **2016**, *7*, 3290–3293. https://doi.org/10.1021/acs.jpclett.6b01316.

(39) Schultz, B.-J.; Mohrmann, H.; Lorenz-Fonfria, V. A.; Heberle, J. Protein Dynamics Observed by Tunable Mid-IR Quantum Cascade Lasers across the Time Range from 10 Ns to 1 S. *Spectrochim. Acta - Part A Mol. Biomol. Spectrosc.* **2017**, *188*, 666 – 674. https://doi.org/10.1016/j.saa.2017.01.010.

(40) Fourmond, V.; Greco, C.; Sybirna, K.; Baffert, C.; Wang, P.-H.; Ezanno, P.; Montefiori, M.; Bruschi, M.; Meynial-Salles, I.; Soucaille, P.; et al. The Oxidative Inactivation of FeFe Hydrogenase Reveals the Flexibility of the H-Cluster. *Nat. Chem.* **2014**, *6* (4), 336–342. https://doi.org/10.1038/nchem.1892.

(41) Goldet, G.; Brandmayr, C.; Stripp, S. T.; Happe, T.; Cavazza, C.; Fontecilla-Camps, J. C.; Armstrong, F. A. Electrochemical Kinetic Investigations of the Reactions of [FeFe]-Hydrogenases with Carbon Monoxide and Oxygen: Comparing the Importance of Gas Tunnels and Active-Site Electronic/Redox Effects. *J. Am. Chem. Soc.* **2009**, *131* (41), 14979–14989. https://doi.org/10.1021/ja905388j.

(42) Camara, J. M.; Rauchfuss, T. B. Combining Acid–base, Redox and Substrate Binding Functionalities to Give a Complete Model for the [FeFe]-Hydrogenase. *Nat. Chem.* **2012**, *4* (1), 26–30. https://doi.org/10.1038/nchem.1180.

(43) Schilter, D.; Camara, J. M.; Huynh, M. T.; Hammes-Schiffer, S.; Rauchfuss, T. B. Hydrogenase Enzymes and Their Synthetic Models: The Role of Metal Hydrides. *Chem. Rev.* **2016**, *116* (15), 8693–8749. https://doi.org/10.1021/acs.chemrev.6b00180.

(44) Möller, F.; Piontek, S.; Miller, R. G.; Apfel, U.-P. From Enzymes To Functional Materials - Towards Activation Of Small Molecules. *Chem. - A Eur. J.* **2017**, *24* (7), 1471–1493. https://doi.org/10.1002/chem.201703451.

(45) Mebs, S.; Kositzki, R.; Duan, J.; Kertess, L.; Senger, M.; Wittkamp, F.; Apfel, U.-P.; Happe, T.; Stripp, S. T.; Winkler, M.; et al. Hydrogen and Oxygen Trapping at the H-

Cluster of [FeFe]-Hydrogenase Revealed by Site-Selective Spectroscopy and QM/MM Calculations. *Biochim. Biophys. Acta - Bioenerg.* **2018**, *1859* (1), 28–41. https://doi.org/10.1016/j.bbabio.2017.09.003.

(46) Stripp, S. T.; Happe, T. How Algae Produce Hydrogen - News from the Photosynthetic Hydrogenase. *Dalt. Trans.* **2009**, *45*, 9960–9969. https://doi.org/10.1039/b916246a.

(47) Ghirardi, M. L.; Posewitz, M. C.; Maness, P.-C.; Dubini, A.; Yu, J.; Seibert, M. Hydrogenases and Hydrogen Photoproduction in Oxygenic Photosynthetic Organisms. *Annu. Rev. Plant Biol.* **2007**, *58* (1), 71–91. https://doi.org/10.1146/annurev.arplant.58.032806.103848.

(48) Swanson, K. D.; Ratzlo, M. W.; Mulder, D. W.; Artz, J. H.; Ghose, S.; Ho, A.; White, S.; Zadvornyy, O. A.; Broderick, J. B.; Bothner, B.; et al. [FeFe]-Hydrogenase Oxygen Inactivation Is Initiated at the H Cluster 2Fe Subcluster. *J. Am. Chem. Soc.* **2015**, *137* (5), 1809–1816. https://doi.org/10.1021/ja510169s.

(49) Albracht, S. P. J.; Roseboom, W.; Hatchikian, E. C. The Active Site of the [FeFe]-Hydrogenase from Desulfovibrio Desulfuricans. I. Light Sensitivity and Magnetic Hyperfine Interactions as Observed by Electron Paramagnetic Resonance. *J. Biol. Inorg. Chem.* **2006**, *11* (1), 88–101. https://doi.org/10.1007/s00775-005-0039-8.

(50) Mebs, S.; Duan, J.; Wittkamp, F.; Stripp, S. T.; Happe, T.; Apfel, U. P.; Winkler, M.; Haumann, M. Differential Protonation at the Catalytic Six-Iron Cofactor of [FeFe]-Hydrogenases Revealed by 57 Fe Nuclear Resonance X-Ray Scattering and Quantum Mechanics/Molecular Mechanics Analyses. *Inorg. Chem.* **2019**, *58*, 4000–4013. https://doi.org/10.1021/acs.inorgchem.9b00100.

ToC Figure

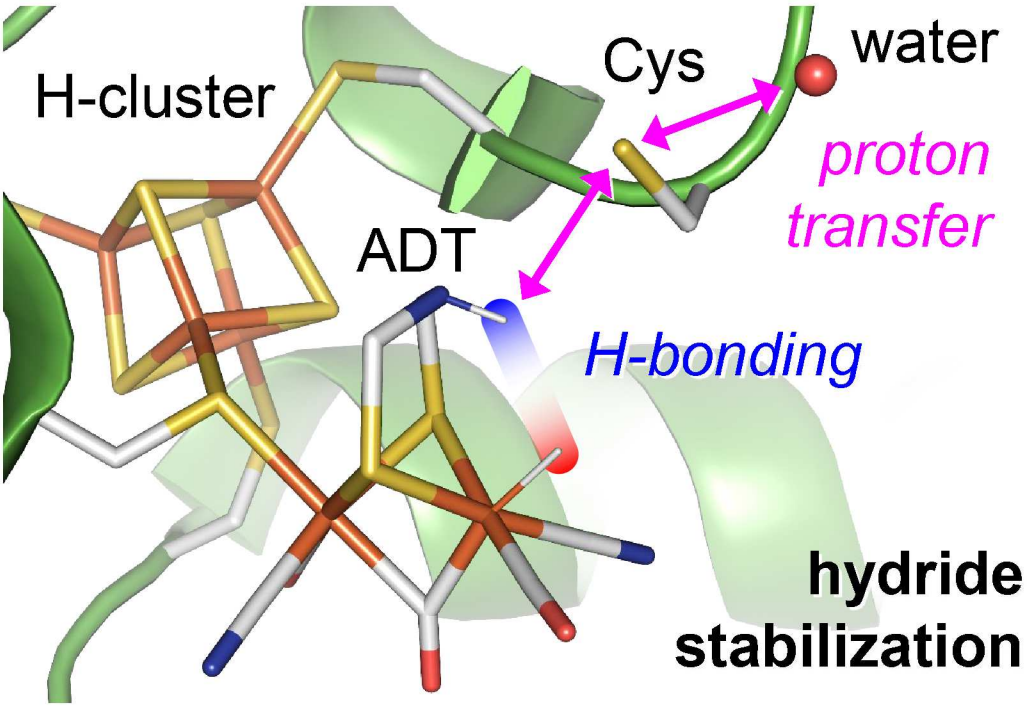

The geometry of the catalytic active site in [FeFe]-hydrogenases is determined by hydrogen bonding and proton transfer.